Article:
Li, J, An, Z, Hage, FS et al. (5 more authors) (2019) Solute clustering and precipitation in an Al–Cu–Mg–Ag–Si model alloy. Materials Science and Engineering: A, 760. pp. 366-376. ISSN 0921-5093

https://doi.org/10.1016/j.msea.2019.06.021

Solute clustering and precipitation in an Al-Cu-Mg-Ag-Si model alloy

Jiehua Li[1]*, Zhiheng An[2], Fredrik S. Hage[3], Huiyuan Wang[4], Pan Xie[1], Shenbao Jin[2], Quentin M. Ramasse[3, 5], Gang Sha[2]*

[1] Institute of Casting Research, Montanuniversität Leoben, Leoben, A-8700, Austria

[2] School of Materials Science and Engineering, Nanjing University of Science and Technology, Nanjing, 210014, PR China

[3] SuperSTEM Laboratory, SciTech Daresbury Campus, Keckwick Lane, Daresbury, WA4 4AD, UK

[4] Key Laboratory of Automobile Materials of Ministry of Education, School of Materials Science and Engineering & International Center of Future Science, Jilin University, No. 5988 Renmin Street, Changchun 130025, PR China

[5] School of Physics and Astronomy and School of Chemical and Process Engineering, University of Leeds, Leeds LS2 9JT, UK

*Corresponding Author. Post address: Institute of Casting Research, Montanuniversität Leoben, A-8700, Leoben, Austria.

Tel.: +43-3842-402-3304; Fax: +43-3842-402-3302.

Email address: **jiehua.li@unileoben.ac.at** (Jiehua Li), **gang.sha@njust.edu.cn** (Gang Sha)

Abstract

Solute clustering and precipitation in an Al-Cu-Mg-Ag-Si model alloy has been investigated by atom probe tomography (APT) as well as high-angle annular dark-field (HAADF) imaging and electron energy loss spectroscopy (EELS) in the scanning transmission electron microscope (STEM). Nine types of solute clusters (Cu, Ag, Mg-Cu, Mg-Ag, Mg-Cu-Si, Mg-Ag-Si, Mg-Ag-Cu, Cu-Ag-Si and MgAgCuSi) were observed by APT in both the as-quenched alloy and after ageing the alloy at 180 °C for 1 h. Three types of precipitates (Ω

(AlCuMgAg), θ (Al_2Cu) and Mg_2Si) were observed by APT and HAADF-STEM after further ageing at 180 °C for 24 h and 100 h. We propose that MgAgCu and MgAgCuSi clusters are likely to be responsible for the formation of the Ω (AlCuMgAg) phase. Furthermore, we also suggest that the θ (Al_2Cu) phase forms from Cu clusters and the Mg_2Si phase forms from the decomposition of MgAgSi and MgAgCuSi clusters by losing Ag to Ω phase growth. Many early binary clusters (Mg-Cu, Mg-Ag) do not seem to undergo a significant further growth during ageing; these are more likely to be transformed into complex ternary and quaternary clusters and be subsequently consumed during the growth of large clusters / precipitates. Furthermore, it is proposed that the plate-like Ω (AlCuMgAg) precipitates evolve continuously from the MgAgCu and MgAgCuSi clusters, rather than via heterogeneous nucleation on their precursors (i.e. MgAgCu and MgAgCuSi clusters). More interestingly, even after ageing at 180 °C for 100 h, the Ω (AlCuMgAg) precipitates remain coherent with the α-Al matrix, indicating that these precipitates have a high thermal stability. This can mainly be attributed to the presence of a single Mg-Ag-rich monolayer observed at the interface between the Ω precipitate and the α-Al matrix, significantly improving the coarsening resistance of the Ω (AlCuMgAg) precipitates. Our results thus reveal links between a variety of solute clusters and the different types of precipitates in the Al-Cu-Mg-Ag-Si model alloy. Such information can in the future be used to control the precipitation by tailoring solute clustering.

Keywords: Al alloy; Solute clustering; Precipitation; HAADF-STEM; Atom probe tomography

1. Introduction

High-performance Al alloys have been widely used in the aerospace and automotive industries. Al is regarded as the second most important metal next to steel because of its relatively low processing costs, its light weight and its ability to be heat treated to fairly high strengths. Cluster and precipitation hardening occurs very often during heat treatment, resulting in strengthening effects for high-performance Al alloys [1-3]. Accurate tailoring of solute clustering and precipitation is crucial for improving the performance of Al alloys, in particular at elevated temperatures. This approach has been widely used in the development of Al-Cu [4-6], Al-Cu-Mg [7-13], Al-Cu-Sn [14-16], Al-Mg-Si [17-21] and Al-Zn-Mg-Cu [22-24] alloys. The Al-Cu-Mg-Ag system in particular [25-48] has been developed as a high strength Al alloy thanks to plate-like Ω (AlCuMgAg) and θ (Al_2Cu) precipitates habiting on the {111} and {001} planes, respectively. More specifically, its high strength and thermal stability have been attributed to the peculiar crystallography of the Ω precipitate, and in particular its propensity for interfacial segregation. Using high-angle annular dark-field (HAADF) imaging and energy-dispersive X-ray spectroscopy (EDX) as well as electron energy loss spectroscopy (EELS) in the scanning transmission electron microscope (STEM), two layers of Ag and Mg segregation were observed on the surfaces of the broad faces of the Ω plates [27, 38], which are believed to relieve the coherent strain at the α-Al / Ω interface. However, solute clustering is hard to observe using HAADF-STEM imaging and EDX or EELS mapping alone due to their limited sensitivity to low dopant levels [27, 38]. In order to elucidate solute clustering, the very high sensitivity of atom probe tomography (APT) was used to reveal that the Ω phase may evolve from co-clusters in a mechanism not involving the segregation of Mg and Ag at the interface of α-Al / Ω [39]. To date, however, a systematic research on how many types of clusters are able to form in the alloy is lacking. More importantly, it is also unclear which solute clusters are responsible for subsequent precipitation of a particular precipitation phase.

Furthermore, coarsening of precipitates can cause the loss of their strengthening effect in Al alloys under extreme service conditions. Achieving an improvement in the coarsening resistance remains a significant research challenge for the international materials community. One of the most important approaches to overcome the coarsening-induced softening problem in precipitation-hardening Al alloys is to increase the number density and coherence level of precipitates within the α-Al matrix [49]. This requires successfully tailoring solute clustering, thereby controlling precipitation as well as engineering the precipitates / Al matrix interfaces in order to develop novel high-performance Al alloys.

In this paper, an Al-Cu-Mg-Ag-Si model alloy is used to investigate solute clustering and precipitation with an enhanced coarsening resistance via a thorough atomic scale experimental characterisation including both APT and HAADF-STEM imaging as well as EELS in the STEM. The main goal of this combined approach is to gain insights into solute clustering and precipitation as well as to understand the effect of the interface structure and the composition of precipitates on their coarsening resistance at elevated temperatures. A special focus is placed on the link between solute clustering and subsequent precipitation. Such information will be useful to guide the design and development of novel high-performance Al alloys.

2. Experimental

The model Al–4.0Cu–0.3Mg–1.0Ag–0.1Si alloy (wt. %, used through this paper unless specified otherwise) was prepared from high purity Al (99.9998%), Cu (99.99%), Mg (99.9%), Ag (99.99%) and Si (99.999%). The composition was measured by inductively coupled plasma optical emission spectrometry (ICP-OES). It should be noted here that the addition of a higher amount of Ag (1.0 wt. %) than commonly used in commercial Al alloys is mainly aimed at elucidating the solute co-clustering of Ag, Mg and Cu. It should also be noted that Si is also added (about 0.1 wt.%) in order to provide a more meaningful comparison with results obtained from commercial purity Al alloys where Si is typically present as an impurity.

Solution treatment was done in a salt bath at 515 °C for 5 h, followed by quenching into cold water and then ageing in oil at 180 °C for up to 100 h. Vickers hardness testing was performed using a LECO Hardness Tester (LV700AT) with a load of 10 N and a dwell time of 15 s. Each data point reported in Fig. 1 represents an average of at least 10 measurements. Error bars in the age-hardening curve represent the standard deviations.

The specimens for TEM investigation were mechanically ground, polished to a thickness of 70 µm, dimpled to 30 µm, and then ion-beam milled (voltage: 4 kV and angle: 4°) using a Gatan Precision Ion Polishing System (PIPS, Gatan model 691). HAADF-STEM images and STEM-EELS spectrum images were acquired using either a Nion UltraSTEM100 (Figs. 11-13) or Nion UltraSTEM100MC (Fig. 14) aberration corrected dedicated STEM. Both microscopes were operated at an acceleration voltage of 100 kV and an electron probe convergence semi-angle of 31 mrad, resulting in an estimated minimum electron probe size of 0.8 Å. Before these detailed HAADF-STEM and EELS measurements, the samples were pre-checked using a FEI Tecnai F20 operated at 200 kV, to determine their suitability in terms of thickness and tilting angles to the $<011>_{Al}$ and $<112>_{Al}$ desired for the atomic-resolution investigations and to provide wider field of view, low magnification images of the entirety of the sample. The thickness measurements were carried out using the standard low loss EELS method [50].

The Nion UltraSTEM100 is equipped with a Gatan Enfina EEL spectrometer, while the Nion UltraSTEM100MC is equipped with a Gatan Enfinium ERS EEL spectrometer. The spectrometer collection semi-angle were 36 mrad and 44mrad, respectively. HAADF detector semi-angles were 83 - 185 mrad (UltraSTEM100) and 85 – 185 mrad (UltraSTEM100MC). Both microscopes have cold field emission guns with a native energy spread of 0.35 eV. In order to optimise the signal-to-noise ratio in the STEM-EELS maps, all EELS spectrum images were de-noised (post-acquisition) using Principal Component Analysis (PCA) as implemented in the MSA plugin [51] for Gatan's Digital Micrograph software. Visual

inspections of components (included and excluded) and residuals were carried out to ensure no obvious structural information was being removed from the reconstruction. The numbers of components included in the reconstructions are as follows: 5 (Fig. 12c-g), 10 (Fig, 12j-n), 5 (Fig. 13c-f) and 4 (Fig. 14d-e and h-j). After subtracting the preceding decaying background (using a power law model) for the following edges (onsets are indicated in brackets): Ag $M_{4,5}$ (367 eV), Cu $L_{2,3}$ (931 eV), Mg K (1305 eV), Al K (1560 eV) [52], EELS maps were created for each edge by integration over a ≈ 50 eV energy window from each edge onset. The intensities of the individual EELS maps are displayed on a grey-scale, while the intensities of the "combined" colour-coded EELS maps are displayed on a false colour scale: a lower (relative) elemental concentration results in a low intensity (black), while an increase in (relative) elemental concentrations results in an increased contrast (colour).

The samples for atom probe analysis were cut and mechanically ground to square rods of approximately 0.5 mm × 0.5 mm × 15 mm, and then sharpened by two-stage micro-electro-polishing. The first stage electropolishing was performed using an electrolyte containing 30 volume percent (vol. %) perchloric acid in acetic acid at 20 V and room temperature. The second stage electropolishing was performed using a 5 vol. % perchloric acid in 2-butoxyethanol solution at 15 V. The APT experiments were performed on a LEAP4000X SI local electrode atom probe at a specimen temperature of 20 K and under an ultra-high vacuum of 3×10^{-11} Torr using a pulse repetition rate of 200 kHz. The UV laser pulse energy is 40-100 pJ and a target evaporation rate is 0.5%. The UV laser energy in this range had no significant influence on the measured alloy composition. A high laser energy improved yield in data collection; here, possible over-heating of the specimen tip was deemed insignificant as the spatial resolution of the laser-pulsed dataset was excellent with pole and zone lines clearly resolved in desorption maps, strongly indicating that the laser energy of 40-100 pJ is suitable for this alloy. Data reconstruction and statistical analyses were performed using Imago Visualization and Analysis Software (IVAS 3.6.8).

Solute clusters in APT reconstructions were identified using a maximum separation algorithm [53]. In this approach, the results of the cluster analysis are strongly dependent on the following two parameters: d-max, whereby any pairs of solute atoms separated by a distance less than the d-max value are identified as a part of the same cluster; and N-min, whereby atoms in the resulting clusters consisting of fewer than N-min atoms are classified as matrix atoms and thus discarded. In the present investigation, d-max and N-min values were determined for all APT datasets using the calibration procedure suggested in Ref. [54]. In addition to d-max and N-min, further parameters (L (envelope parameter, nm), E (erosion distance, nm)) for cluster analysis are listed in Table 1. It should be noted here that many previous studies, for instance in Ref. [55], have focused on measuring the precise 'whole', or absolute composition of each cluster. Such measurements are known to be very sensitive to all the cluster identification parameters d-max, N-min, L and E. Although significant efforts were made to optimize cluster identification parameters to get accurate results, the uncertainty in these earlier measurements remains undetermined. This is because the trajectory overlap in APT experiments between precipitate and matrix species is hard to estimate accurately, especially for the smallest clusters. In the present work, we use a different approach in our cluster analysis: we focused on clustered solute atoms in isolation without taking into consideration solvent atoms that are also found in the matrix, i.e. we aimed to determine a cluster's relative solute concentration rather than its absolute concentration within the entire system. The advantage of our approach is that the cluster identification is mainly sensitive to d-max and N-min, and only slightly to L, but is insensitive to E (see appendix Table S1 and S2 for a comparison of results obtained by choosing with different values of E). This approach allowed us to differentiate between cluster types based on the relative solute composition (of each cluster) and to work out their number density and their relative sizes. Using this information, we can deduce how each cluster type evolved during ageing. Such an approach has been shown to reliably provide valuable information for understanding

clustering and precipitation pathways in many previous publications [10, 12, 19, 56]. The relative solute composition of clusters, the number of each cluster type, cluster quantity fraction (%) and mean size (number of solute atoms) were calculated based on the cluster analysis results, listed in Table 2.

3. Results

3.1 Age hardening response

Fig. 1 shows the age hardening response of the Al–4.0Cu–0.3Mg–1.0Ag–0.1Si alloy through annealing at 180 °C up to 100 h. The hardness of the as-quench (AQ) sample is about 115 HV. The hardness decreases with increasing ageing time up to 1 h. Then the hardness increases gradually and reaches the peak hardness (155 HV) after 24 h. Further ageing up to 100 h leads to over-ageing and a progressive decrease in hardness. On the basis of this age hardening response, four samples aged at 0 h (AQ), 1 h, 24 h and 100 h were selected for further atomic scale experimental characterization of solute clustering (AQ and sample aged at 1 h) and subsequent precipitation (sample aged at 24 h and 100 h).

3.2 Solute clustering by APT examinations

Fig. 2 shows the 3D reconstructions of atoms maps including solute clusters in the Al–4.0Cu–0.3Mg–1.0Ag–0.1Si alloy in AQ condition. By a visual examination of these APT reconstructions, the distributions of the solutes (Al, Cu and Si) appear to be more or less uniform in the AQ sample. However, a nearest-neighbour analysis, as shown in Fig. 3, indicates that Cu, Mg, Ag and Si in fact developed non-random distributions in the AQ sample. Clusters with Cu, Mg, Ag and Si target solute atoms were identified using the parameters described in section 2. As described above, these are defined as clusters that have grown beyond a critical size during thermal ageing, rather than small “random” aggregates of the target solute atoms that have failed to grow into larger sizes and are highly likely to be

present in the alloy with solute atoms in uncorrelated distributions. This critical size is determined to be N-min = 7 solute atoms, from the size of the largest clusters detected in the regenerated datasets with solute atoms in random distributions. Random clusters are subsequently ignored in the analysis, with only the larger clusters believed to further evolve or transform into precipitates (with sizes much larger than the non-random solute clusters). The clusters are then grouped into types based on their relative composition, and their numbers (absolute and relative to the total number of clusters) are then tabulated (see Tables S1 and S2). The filtered results reveal that there exist nine different cluster types (Cu, Ag, MgCu, MgAg, MgCuSi, MgAgSi, MgAgCu, CuAgSi and MgAgCuSi) in AQ condition. Among these clusters, the Cu, MgCu and MgAgCu clusters are the most numerous, while CuAg and MgAgCuSi clusters are second in predominance. Interestingly, all these early solute clusters have a similar average size (8 – 10 atoms, Table 2) in the AQ sample. The cluster analysis was conducted using high-quality data in a box of 40 × 40 × 100 nm^3 selected from the APT analysis volume (without poles and zone lines) using the parameters listed in Table 1. The average composition, number, cluster quantity fraction (%) and mean size (solute atom number) of the six most numerous cluster types (Cu, MgCu, CuAg, MgCuSi, MgAgCu, MgAgCuSi) are given in Table 2. It should be noted here that due to the time-consuming nature of these experiments, the values in Table 2 are only representative of the relatively modest observed volume: a full statistical analysis of the alloy using many APT needles may provide the basis for further work.

Fig. 4 shows 3D APT reconstructions of atom maps including solute clusters in an Al–4.0Cu–0.3Mg–1.0Ag–0.1Si alloy sample, aged at 180 °C for 1 h. Similar to the AQ condition sample, the cluster analysis was also conducted using high quality data in a box of 40 × 40 × 100 nm^3 selected from the APT analysis volume (without poles and zone lines) using the parameters listed in Table 1. Upon visual inspection, the presence of Ag-rich clusters appears more obvious in the sample aged at 180 °C for 1 h than in the AQ sample. Furthermore, Fig. 4

shows that these Ag-rich clusters are also enriched in Mg and Cu, which can be seen more clearly in Figure 5. Similar to Fig. 3, Fig. 6 shows the nearest-neighbour analysis, clearly indicating that Cu, Mg, Ag and Si developed non-random distributions after 1 h of ageing. Six types of cluster populations remain predominant after the 1 h ageing process. Compared to the AQ sample, the Mg concentration in the MgCu, MgAgCu and MgAgCuSi clusters is increased, the Ag concentration in the CuAg, MgAgCu and MgAgCuSi clusters is increased, and the Si and Cu concentrations in the MgCuSi clusters are also increased. After ageing at 180 °C for 1 h, the number density of all clusters becomes higher, with the exception of the number density of MgCu clusters, which appears to decrease, as shown in Table 2 (number of clusters). The size of all clusters increases, as shown in Table 2 (number of atoms), with two exceptions: the sizes of the MgCu and CuAg clusters appear to be smaller, which may be due to the fact that the MgCu and CuAg clusters may turn into MgAgCu clusters through the partitioning of Mg and Ag. Interestingly, three types of Ag-containing clusters, i.e. MgAgCu, MgAgSi and MgCuAgSi, show a very significant increase in their average size, which is fully consistent with the suggestion that clusters are not an equilibrium phase, instead they are dynamic in nature and evolve with ageing time. The composition of each solute cluster is assumed to be evolving, likely with the help of vacancy-assisted diffusion. In this sense, all solute clusters exhibit a transient random fluctuation, which should not be seen as an artefact in the measurements.

3.3 APT examinations of the precipitation behaviour

Fig. 7 shows 3D reconstructions of atoms maps including precipitates in an Al–4.0Cu–0.3Mg–1.0Ag–0.1Si alloy, aged at 180 °C for 24 h. After ageing at 180 °C for 24 h, three different types of precipitates (Ω (AlCuMgAg), θ (Al_2Cu) and Mg_2Si) are now observed. Fig. 8 shows a more detailed analysis of these precipitates. The quantitative analysis of θ (Al_2Cu) and Mg_2Si is shown in Fig. 8b and 8c, respectively. The analysis of Ω (AlCuMgAg) in the

sample aged for 24 h is not shown here because a similar analysis was performed for the sample aged for 100 h, as shown in Figs. 9, 10.

Similar to the sample aged for 24 h, as shown in Figs. 7 and 8, these three types of precipitates (Ω (AlCuMgAg), θ (Al_2Cu) and Mg_2Si) were also observed after ageing at 180 °C for 100 h, as shown in Fig. 9. Consistent with observations reported in the literature [27, 38, 39], a Mg-Ag-rich region was observed to be present within the Ω (AlCuMgAg) precipitates, which can be more clearly seen from a more detailed analysis shown in Fig. 10b, d. Furthermore, the Mg_2Si phase appears to be systematically positioned in the vicinity of the Ω (AlCuMgAg) precipitates, which can be more clearly seen from Fig. 10d, e. When compared with Fig. 7 and Fig. 9, the size of the Ω precipitates is much smaller than that of θ (Al_2Cu), which can be more clearly seen by comparing the Cu and Ag maps in Figs. 7, 9 because Cu is present in Ω (AlCuMgAg) and θ (Al_2Cu), while Ag is only present in Ω (AlCuMgAg). Furthermore, the number density of the Ω precipitate appears to be much higher than that of θ (Al_2Cu). However, the analysis of number density based on the APT results is merely indicative as the volume measured by APT is relatively small (about 10000 nm^3), while the volume of precipitates (Ω (AlCuMgAg) and θ (Al_2Cu)) themselves is relatively large (about 500 nm^3).

3.4 **Examination of the precipitation behaviour by HAADF-STEM and EELS**

In order to probe larger samples regions, low magnification annular dark field STEM images were used for an additional measurement of number density. While this enabled more than 200 precipitates to be counted and classified across a number of distinct regions of the sample, the intrinsically small volumes probed by electron microscopy, along with unavoidable projection and depth of field effects, mean that this determination of number density remains approximate: a fully representative analysis would require the use of another correlative

technique such as small angle X-ray scattering, which is beyond the scope of this work. As the habit plane of Ω (AlCuMgAg) is on the $\{111\}_{Al}$ plane, and the habit plane of θ (Al_2Cu) is on the $\{001\}_{Al}$ plane [27, 38, 39], the sample was examined along the $<011>_{Al}$ zone axis, as shown in Fig. 11. The thickness of the regions used for this analysis was estimated to be about 50 ± 5 nm using EELS, as described in section 2. The number density of Ω (AlCuMgAg) precipitates was measured to be $2.3 \pm 0.2 \times 10^{24}$ m^{-3}, which is 5 times of that ($0.45 \pm 0.1 \times 10^{24}$ m^{-3}) of θ (Al_2Cu) precipitates.

At higher magnification, a careful examination of the atomic-resolution HAADF-STEM images in Fig. 12, acquired along $<011>_{Al}$ and $<112>_{Al}$, reveals the presence of one Mg-Ag-rich monolayer at the interface between the Ω precipitate and the α-Al matrix. When viewed along $<112>_{Al}$ (Fig. 12a-g), the Ω (AlCuMgAg) precipitates are fully coherent with α-Al matrix. The orientation relationship between the Ω precipitate and the α-Al matrix can be indexed as $<112>_{\Omega}$ $\{001\}_{\Omega}$ // $<112>_{Al}\{001\}_{Al}$. When viewed along a $<011>_{Al}$ zone axis (Fig. 12h-n), the Ω (AlCuMgAg) precipitates are again fully coherent with the α-Al matrix, with one Mg-Ag-rich monolayer clearly resolved at each interface. It should be noted here that no significant thickening ledges on Ω (AlCuMgAg) precipitates were observed, as illustrated in Fig. 12, which shows a representative example of all the precipitates observed in this sample.

Using the same methodology as for the sample aged at 180 °C for 24 h, low magnification HAADF-STEM images were also acquired along $<011>_{Al}$ for the sample aged at 180 °C for 100 h. The number density of Ω (AlCuMgAg) precipitates in the sample aged at 180 °C for 100 h was measured to be $3.8 \pm 0.21 \times 10^{23}$ m^{-3}, which is close to that ($3.6 \pm 0.15 \times 10^{23}$ m^{-3}) of the θ (Al_2Cu) precipitates. Clearly, within the measurement error, the number density of both Ω (AlCuMgAg) and θ (Al_2Cu) precipitates decreases with increasing the ageing time from 24 h to 100 h. However, the ratio of θ (Al_2Cu) to Ω (AlCuMgAg) increases from 0.2 to 1 upon increasing the ageing time from 24 h to 100 h. Interestingly, even after ageing at 180 °C

up to 100 h, the Ω (AlCuMgAg) precipitates still remain coherent with the Al matrix, as viewed from the atomic-resolution images obtained in $<001>_{Al}$ (Figs. 13) and $<112>_{Al}$ (Fig. 14) projections. After this longer ageing treatment, HAADF images of some Ω (AlCuMgAg) precipitates exhibited features that are consistent with the presence of 'thickening ledges'; this is illustrated in Fig. 13a. This stands in contrast to HAADF images of Ω (AlCuMgAg) precipitates in the 24 h aged sample, where no indication of thickening ledges was observed (within the limited field of observation intrinsic to atomic-resolution work). It should be noted here that only a small number of precipitates were observed to possess this thickening ledge, and due to the relatively small volume probed by STEM-EELS, this observation may need to be investigated further. Similar to the sample aged at 180 °C for 24 h, one Mg-Ag-rich monolayer is present on the interfaces between Ω precipitates and the surrounding Al matrix, as shown in Fig. 14. The observation of the Mg-Ag-rich monolayer (Fig. 14) is fully consistent with the APT results (Fig. 10), which suggested the co-location of Mg, Cu and Ag. The STEM-EELS results provide complementary information since it is hard to accurately determine using APT whether Mg and Ag segregate the interior of the precipitate or at the interface with the Al matrix, due to the relatively poor (~ 0.5 nm) lateral (x - y plane) resolution of APT .

4. Discussion

4.1 Correlation between solute clustering and precipitation

Nine types of solute clusters (Cu, Ag, Mg-Cu, Mg-Ag, Mg-Cu-Si, Mg-Ag-Si, Mg-Ag-Cu, Cu-Ag-Si and MgAgCuSi) were identified by APT in the AQ sample and after ageing at 180 °C for 1 h. When increasing the ageing time up to 100 h, three different types of precipitates (Ω (AlCuMgAg), θ (Al_2Cu) and Mg_2Si) were observed. It is well-accepted that in the Al-Cu-Mg alloy system, apart from the θ (Al_2Cu) phase, other types of precipitates (i.e. the S-Al_2CuMg phase) may also be present, depending on the ratio of Cu:Mg and the ageing temperature. In

the present Al-Cu-Mg-Ag-Si alloy system, no S-Al_2CuMg phase was observed; instead only the Ω (AlCuMgAg) and θ (Al_2Cu) phases were observed, indicating that the presence of Ag may change the precipitation path by inhibiting the formation of the S-Al_2CuMg phase or promoting the formation of Ω (AlCuMgAg). As determined by APT (Fig. 2 and Fig. 4) and subsequent clustering analysis (Table 2), in the AQ sample, Cu, MgCu and MgAgCu clusters are the top three predominant population types. Subsequently, there may be a competition between Cu, MgCu and MgAgCu clusters during further ageing. For example, Cu clusters may act as precursors for θ (Al_2Cu) without further involvement of Mg and Ag. MgCu clusters are known to grow into the S-Al_2CuMg phase with a further partitioning of Cu and Mg. In the present investigation, however, the significant MgAgCu clustering observed and the lack of observation of any S-phase precipitate are attributed to the large amount of added Ag (1 wt. %). Furthermore, CuAg and MgAgCuSi clusters were also observed to be second in predominance with respect to the first group of clusters (Cu, MgCu and MgAgCu), which strongly indicates that Ag is very likely to form a co-cluster with Cu. Ag therefore appears to exhibit a very significant clustering behaviour. It can be proposed that, on the one hand, the partitioning of Ag into Cu and / or CuMg clusters inhibits the formation of MgCu clusters and therefore prevents the formation of the S-Al_2CuMg phase. On the other hand, the partition of Ag into Cu and / or CuMg clusters promotes the formation of MgAgCu clusters and CuAg clusters, and thereby the formation of the Ω (AlCuMgAg) phase. It should be noted here that the partition of Ag into Cu and / or CuMg clusters is a diffusion-controlled process. At the very early stages of ageing, Cu clusters may still be a dominant cluster type and therefore a plentiful ‘reservoir’ of Cu clusters is available for the formation of θ (Al_2Cu). This suggestion can be further supported by previous reports that Cu clusters tend to evolve from an initial spherical morphology to preferentially lie on $\{200\}_{Al}$ planes [4] (which is also the habit plane of θ (Al_2Cu)). Table 2 shows that the Mg concentration in MgCu, MgAgCu and MgAgCuSi clusters increases with increasing ageing time. More importantly, the Ag concentration in the

CuAg, MgAgCu and MgAgCuSi clusters also increases. Likewise, the Mg and Ag concentrations increase in the MgCu clusters with increasing ageing. This strongly indicates that, with the involvement of Ag, MgCu clusters will eventually grow into MgCuAg clusters and form Ω (AlCuMgAg), rather than the S-Al_2CuMg phase. This is fully consistent with the absence of the S-Al_2CuMg phase in the present investigation and a previous report that MgAgCuSi clusters tend to evolve from an initial spherical morphology to preferentially lie on $\{111\}_{Al}$ planes [4] (which is the habit plane of Ω (AlCuMgAg)). Regardless, the number and average size (solute atom number) of MgCu clusters will decrease, which is also consistent with our present clustering analysis, as listed in Table 2.

Apart from the partition of Ag into Cu and / or CuMg clusters, another important factor affecting the precipitation path is the partition of Si into MgCuSi clusters. Although the relative Si concentration is lower (0.1 wt. %) than those of the main alloying elements (Cu, Mg, Ag), Mg_2Si precipitates were often observed in the vicinity of the Ω (AlCuMgAg) precipitates, as shown in Figs. 8, 10. As listed in Table 2, the concentration of Si in MgCuSi clusters increases with increasing ageing time up to 1 h. In addition, there may also be a competition between the formation of MgCuSi and MgCuAg clusters depending on the partition potency of Ag and Si into MgCu, respectively. Alternatively, it is also possible that the partitioning of both Ag and Si into MgCu clusters occurs simultaneously and promotes the formation of Ω (AlCuMgAg) and Mg_2Si precipitates. This would also be fully consistent with our APT results in Figs. 8, 10, which show that Mg_2Si precipitates are always present in the vicinity of the Ω (AlCuMgAg) phase.

Apart from the above clusters composition analysis, a very simple analysis of average cluster size can also confirm that MgAgCu and MgAgCuSi clusters are likely to be responsible for the formation of the Ω phase, and that Mg_2Si is likely to form from the decomposition of MgAgSi and MgAgCuSi clusters by losing Ag to Ω phase growth. Indeed, as listed in Table 2, a significant initial growth of three types of Ag-containing clusters (i.e. MgAgCu, MgAgSi

and MgAgCuSi) through the consumption of the early binary clusters was observed. However, the solute clustering during the early stages of ageing is relatively complicated. In order to elucidate the exact role of different alloying elements during solute clustering, a series of well-designed experiments focusing on the addition of defined alloying elements is required and beyond the scope of the present report. For example, in order to elucidate the possible competition between Si and Ag in MgCu clusters, the two quaternary AlCuMgSi and AlCuMgAg alloy systems need to be investigated. Regardless, the present investigation demonstrates clearly that solute clustering can be linked to subsequent precipitation, thus indicating that control of the precipitation process could be achieved by tailoring the solute clustering process.

4.2 Strengthening effect of solute clusters and precipitates

The hardness of the Al–4.0Cu–0.3Mg–1.0Ag–0.1Si alloy in AQ condition is about 115 HV, which is significantly higher than the 60 HV of the Ag-free Al–1.1Cu–1.7Mg (at. %) alloy [9]. This strongly suggests that a significant solute clustering of Mg, Cu, Si and Ag (most likely as MgAgCu and MgAgCuSi clusters, as discussed above), and thereby clustering hardening, occurs in the alloy upon the addition of Ag. In Al–1.1Cu–1.7Mg (at. %) alloys, it was proposed that pre-precipitate atomic co-clusters of Cu and Mg are responsible for the rapid hardening reaction. By contrast here, in the Al–4.0Cu–0.3Mg–1.0Ag–0.1Si alloy, nine types of solute clusters were observed during the early stages of ageing. A more significant cluster hardening can thus be expected.

Adding Ag into an Al-Cu-Mg alloy with a high Cu / Mg ratio (as in the present investigation) can result in the precipitation of the Ω (AlCuMgAg) phase [26-48]. The Ω (AlCuMgAg) phase, which possesses a long plate-shaped morphology and a relatively higher ratio of length to thickness compared to θ (Al_2Cu), has an orthorhombic crystal structure with a = 0.496 nm, b = 0.859 nm, c = 0.848 nm [41, 43] and precipitates on $\{111\}_{Al}$, unlike θ (Al_2Cu), which has

a $\{100\}_{Al}$ habit plane [5-8]. The θ (Al_2Cu) phase nucleates heterogeneously on dislocations. It is generally accepted that the precipitation of Ω (AlCuMgAg) can increase the tensile strength and hardness of Al-Cu-Mg-Ag alloys (Fig. 1) [37, 40]. More importantly, these Al-Cu-Mg-Ag alloys also exhibit a better creep resistance at high temperatures because the thermal stability of the Ω (AlCuMgAg) precipitate is superior to that of the θ (Al_2Cu) precipitate in Al matrices [26-48]. Here, the observation that the Ω (AlCuMgAg) phase still remains coherent even after ageing at 180 °C up to 100 h (Figs. 13, 14), in contrast to the θ (Al_2Cu) phase, is essential. The strengthening effect of the Ω (AlCuMgAg) phase is thus higher and can remain so for a longer while during ageing. At least one question arises as a result of these considerations: how can we promote the formation of the Ω (AlCuMgAg) precipitates while simultaneously supressing the formation of the θ (Al_2Cu) precipitates? The precipitation of Ω (AlCuMgAg) occurs prior to the precipitation of θ (Al_2Cu) but after the growth of MgAgCu and / or MgAgCuSi clusters [26]. Two possible approaches can be suggested to promote the precipitation of Ω (AlCuMgAg) and simultaneously supress the precipitation of θ (Al_2Cu). The first route would be to tailor the clustering of MgAgCu and / or MgAgCuSi. Possible methods may include: (i) micro-alloying (i.e. adjusting the ratio of Cu / Mg and / or the Ag concentration), (ii) the use of a pre-ageing treatment [29, 48], and (iii) allowing deformation (i.e. rolling) to enhance the formation of more dislocations and vacancies [57], which may result in an increase of the number density and size of MgAgCu and / or MgAgCuSi clusters. The second possible approach consists in suppressing the transformation of Ω (AlCuMgAg) into θ (Al_2Cu), which can be achieved by tailoring the interface structure of Ω (AlCuMgAg) by adjusting ageing parameters (temperature and time). For example, in the present investigation, the ageing was done at 180 °C. As reported in Ref. [27], the thickening of Ω plates is restricted by a limited supply of ledges. After ageing at 180 °C up to 24 h, the density of thickening ledges on Ω plates was very low, usually zero [27]: no thickening ledge was observed here up to 24 h ageing, as illustrated in Fig. 12. By contrast, a small number of Ω

plates with apparent thickening ledges were observed after ageing at 180 °C up to 100 h, as illustrated in Fig. 13a. In fact, the high coarsening resistance of Ω (AlCuMgAg) at temperatures up to 180 °C can be directly attributed to a prohibitively high barrier to ledge nucleation in the strong vacancy field normal to the broad face of the Ω (AlCuMgAg), as reported in [27].

5. Conclusion

Solute clustering and precipitation have been found to produce a significant strengthening effect in an Al-Cu-Mg-Ag-Si alloy during ageing at 180 °C. APT as well as HAADF-STEM and EELS investigations provide new insights into the clustering and precipitation behaviour of solute species in the alloy.

(1) APT results show that nine types of solute clusters (i.e. Cu, Ag, Mg-Cu, Mg-Ag, Mg-Cu-Si, Mg-Ag-Si, Mg-Ag-Cu, Cu-Ag-Si and MgAgCuSi) form in the Al-Cu-Mg-Ag-Si alloy, both in the AQ alloy and in the alloy aged at 180 °C up to 1 h.

(2) MgAgCu and MgAgCuSi clusters are likely to be responsible for the formation of the Ω phase. The θ phase forms from Cu clusters and Mg_2Si forms from the decomposition of MgAgSi and MgAgCuSi clusters by losing Ag to Ω phase growth. Many early binary clusters do not show any significant growth; these are more likely to be transformed into complex clusters and be consumed by the growth of large clusters / precipitates.

(3) An Mg-Ag-rich monolayer forms on the interface between the Ω precipitate and the α-Al matrix. The monolayer significantly improves the coarsening resistance of the Ω (AlCuMgAg) precipitates. Consequently, the Ω (AlCuMgAg) precipitates still remain coherent with the Al matrix and thereby keep their strengthening effect for the alloy even if aged at 180 °C for 100 h.

(4) Tailoring of the solute clustering can be used to control the precipitation process in the Al alloy.

Acknowledgements

J. L. gratefully acknowledges the financial support from the Major International (Regional) Joint Research Project (No. 51420105005), the Overseas, Hong Kong, Macao Scholars Cooperative Research Fund (No. 51728101) from China, EPU 11/2018 and Austrian Science Fund (FWF (P 32378-N37)). The SuperSTEM Laboratory is the U.K. National Research Facility for Advanced Electron Microscopy, supported by the Engineering and Physical Sciences Research Council (EPSRC).

Data Availability

The raw/processed data required to reproduce these findings cannot be shared at this time as the data also forms part of an ongoing study.

References

[1] F.W. Gayle, M. Goodway, Precipitation hardening in the first aerospace aluminium alloy: the wright flyer crankcase, Science. 266 (1994) 1015-1017.

[2] I.J. Polmear, The influence of small additions of silver on the structure and properties of aged aluminium alloys, Journal of Metals. 6 (1968) 44-51.

[3] I.J. Polmear, M.J. Couper, Design and development of an experimental wrought aluminium alloy for use at elevated temperatures, Metallurgical and materials transactions A. 19 (1988) 1027-1035.

[4] V. Fallah, A. Korinek, N. Ofori-Opoku, N. Provatas, S. Esmaeili, Atomistic investigation of clustering phenomenon in the Al–Cu system: Three-dimensional phase-field crystal simulation and HRTEM/HRSTEM characterization, Acta Mater. 61 (2013) 6372-6386.

[5] L. Bourgeois, N. V. Medhekar, A.E. Smith, M. Weyland, J.F. Nie, C. Dwyer, Efficient Atomic-Scale Kinetics through a Complex Heterophase Interface, Physical review letters. 046102 (2013) 1-5.

[6] L. Bourgeois, C. Dwyer, M. Weyland, J.F. Nie, B.C. Muddle, Structure and energetics of the coherent interface between the θ' precipitate phase and aluminium in Al-Cu, Acta Mater. 59 (2011) 7043-7050.

[7] R. Sankaran, C. Laird, Kinetics of growth of plate like precipitates, Acta Metallurgica. 22 (1974) 957-969.

[8] S.P. Ringer, K. Hono, T. Sakurai, I.J. Polmear, Cluster hardening in an aged Al-Cu-Mg alloy, Scripta Mater. 36 (1997) 517-521.

[9] S.P. Ringer, K. Hono, I.J. Polmear, T. Sakurai, Precipitation processes during the early stages of ageing in Al-Cu-Mg alloys, Applied surface science. 94/95 (1996) 253-260.

[10] G. Sha, R.K.W. Marceau, X. Gao, B.C. Muddle, S.P. Ringer, Nanostructure of aluminium alloy 2024: Segregation, clustering and precipitation processes, Acta Mater. 59 (2011) 1659-1670.

[11] M.J. Starink, S.C. Wang, The thermodynamics of and strengthening due to co-clusters General theory and application to the case of Al-Cu-Mg alloys, Acta Mater. 57 (2009) 2376-2389.

[12] R.K.W. Marceau, G. Sha, R. Ferragut, A. Dupasquier, S.P. Ringer, Solute clustering in Al-Cu-Mg alloys during the early stages of elevated temperature ageing, Acta Mater. 58 (2010) 4923-4939.

[13] A. Deschamps, T.J. Bastow, F. de Geuser, A.J. Hill, C.R. Hutchinson, In situ evaluation of the microstructure evolution during rapid hardening of an Al-2.5Cu-1.5Mg (wt.%) alloy, Acta Mater. 59 (2011) 2918-2927.

[14] L. Bourgeois, C. Dwyer, M. Weyland, J.F. Nie, B.C. Muddle, The magic thicknesses of θ' precipitates in Sn-microalloyed Al-Cu, Acta Mater. 60 (2012) 633-644.

[15] S.P. Ringer, K. Hono, T. Sakurai, Nucleation and growth of θ' precipitation in Sn-modified Al-Cu alloys: APFIM / TEM observations, Applied surface science. 87/88 (1995) 223-227.

[16] T. Homma, M.P. Moody, D.W. Saxey, S.P. Ringer, Effect of Sn Addition in Preprecipitation Stage in Al-Cu Alloys: A Correlative Transmission Electron Microscopy and Atom Probe Tomography Study, Metall and Mat Trans A 43 (2012) 2192-2202.

[17] M. Liu, J. Čížek, C.S.T. Chang, J. Banhart, Early stages of solute clustering in an Al–Mg–Si alloy, Acta Mater. 91 (2015) 355-364.

[18] S. Pogatscher, H. Antrekowitsch, H. Leitner, T. Ebner, P.J. Uggowitzer, Mechanisms controlling the artificial aging of Al-Mg-Si Alloys, Acta Mater. 59 (2011) 3352-3363.

[19] R.K.W. Marceau, A. de Vaucorbeil, G. Sha, S.P. Ringer, W.J. Poole, Analysis of strengthening in AA6111 during the early stages of aging: Atom probe tomography and yield stress modelling, Acta Mater. 61 (2013) 7285-7303.

[20] V. Fallah, B. Langelier, N. Ofori-Opoku, B. Raeisinia, N. Provatas, S. Esmaeili, Cluster evolution mechanisms during aging in Al-Mg-Si alloys, Acta Mater. 103 (2016) 290-300.

[21] A. Poznak, R.K.W. Marceau, P.G. Sanders, Composition dependent thermal stability and evolution of solute clusters in Al-Mg-Si analyzed using atom probe tomography, Materials Science and Engineering A, 721 (2018) 47-60.

[22] P.V. Liddicoat, X.Z. Liao, Y.H. Zhao, Y.T. Zhu, M.Y. Murashkin, E.J. Lavernia, R.Z. Valiev, S.P. Ringer, Nanostructural hierarchy increases the strength of aluminium alloys, Nature Communication. 1 (2010) 63 DOI: 10.1038/ncomms1062.

[23] C.R. Hutchinson, F. de Geuser, Y. Chen, A. Deschamps, Quantitative measurements of dynamic precipitation during fatigue of an Al-Zn-Mg-(Cu) alloy using small-angle X-ray scattering, Acta Mater. 74 (2014) 96-109.

[24] P. Schloth, J. N. Wagner, J. L. Fife, A. Menzel, J.-M. Drezet, H. Van Swygenhoven, Early precipitation during cooling of an Al-Zn-Mg-Cu alloy revealed by in situ small angle X-ray scattering, Appl. Phys. Lett. 105, (2014) 101908.

[25] K. Hono, Atom probe microanalysis and nanoscale microstructures in metallic materials, Acta Mater. 47 (1999) 3127-3145.

[26] C. Change, S. Lee, J. Lin, R. Jeng, The Effect of Silver Content on the Precipitation of the Al-4.6Cu-0.3Mg Alloy, Materials Transactions. 46 (2005) 236-240.

[27] C.R. Hutchinson, X. Fan, S. J. Pennycook, G.J. Shiflet, On the origin of the high coarsening resistance of Ω plates in Al-Cu-Mg-Ag alloys, Acta Mater. 49 (2001) 2827-2841.

[28] Y. Zhou, Z. Liu, S. Bai, P. Ying, L. Lin. Effect of Ag additions on the lengthening rate of Ω plates and formation of σ phase in Al-Cu-Mg alloys during thermal exposure, Materials characterization. 123 (2017) 1-8.

[29] S. Bai, X. Zhou, Z. Liu, P. Xia, M. Liu, S. Zeng, Effects of Ag variations on the microstructures and mechanical properties of Al–Cu–Mg alloys at elevated temperatures, Materials science and engineering A. 611 (2017) 69-76.

[30] B.T. Sofyan, K. Raviprasad, S.P. Ringer, Effects of microalloying with Cd and Ag on the precipitation process of Al–4Cu–0.3Mg (wt%) alloy at 200°C, Micro. 32 (2001) 851-856.

[31] K. Raviprasad, C.R. Hutchinson, T. Sakurai, S.P. Ringer, Precipitation processes in an Al-2.5Cu-1.5Mg (wt. %) alloy microalloyed with Ag and Si, Acta Mater. 51 (2003) 5037-5050.

[32] M. Gazizov, R. Kaibyshev, Precipitation structure and strengthening mechanisms in an Al-Cu-Mg-Ag alloy, Materials science and engineering A. 702 (2017) 29-40.

[33] S. Bai, P. Ying, Z. Liu, J. Wang, J. Li, Quantitative transmission electron microscopy and atom probe tomography study of Ag-dependent precipitation of Ω phase in Al-Cu-Mg alloys, Materials science and engineering A. 687 (2017) 8-16.

[34] M. Murayama, K. Hono, Role of Ag and Mg on precipitation of T1 phase in an Al-Cu-Li-Mg-Ag alloy, Scripta Mater. 44 (2001) 701-706.

[35] J.M. Rosalie, L. Bourgeois, Silver segregation to θ' (Al2Cu)-Al interfaces in Al-Cu-Mg alloys, Acta Mater. 60 (2012) 6033-6041.

[36] D. Shin, A. Shyam, S. Lee, Y. Yamamoto, J.A. Haynes, Solute segregation at the Al/θ'-Al2Cu interface in Al-Cu alloys, Acta Mater. 141 (2017) 327-340.

[37] B.M. Gable, G.J. Shiflet, E.A. Starke, Jr. Alloy, Development for the Enhanced Stability of Precipitates in Al-Cu-Mg-Ag Alloys, Metallurgical and materials transactions A. 37 (2006) 1091-1105.

[38] S. Kang, Y. Kim, M. Kim, J. Zuo, Determination of interfacial atomic structure, misfits and energetics of Ω phase in Al–Cu–Mg–Ag alloy, Acta Mater. 81 (2014) 501-511.

[39] L. Reich, M. Murayama, K. Hono, Evolution of Ω phase in an Al-Cu-Mg-Ag alloy: a three-dimensional atom probe study, Acta Mater. 46 (1998) 6053-6062.

[40] J.A. Taylor, B.A. parker, I.J. Polmear, Precipitation in Al-Cu-Mg-Ag casting alloy, Metal science. 10 (1978) 478-482

[41] S. Kerry, V.D. Scott, Structure and orientation relationship of precipitates formed in Al-Cu-Mg-Ag alloys, Metal science. 18 (1984) 289-294.

[42] G. Riontino, Precipitation sequence in an Al-Cu-Mg-Ag-Zn alloy, Philosophical magazine A. 72 (1995) 765-782.

[43] A. Garg, J. M. Howe, Convergent-beam electron diffraction analysis of the Ω phase in an Al-4.0Cu-0.5Mg-0.5Ag alloy, Acta Metall Mater. 39 (1991) 1939-1946.

[44] B.C. Muddle, I.J. Polmear, The precipitation Ω phase in Al-Cu-Mg-Ag alloys, Acta Metall. 37 (1989) 777-789.

[45] V.D. Scott, S. Kerry, R. L. Trumper, Nucleation and growth of precipitates in Al-Cu-Mg-Ag alloys, Materials science and technology. 3 (1987) 827- 835.

[46] J. H. Auld, Structure of metastable precipitate in some Al-Cu-Mg-Ag alloys, Materials science and technology. 2 (1988) 784- 787.

[47] M.K. Knowles, W.M. Stobbs, The structure of {111} age-hardening precipitates in Al-Cu-Mg-Ag alloys, Acta Cryst. 44 (1988) 207-227.

[48] R. Ferragut, A. Dupasquier, C.E. Macchi, A. Somoza, R.N. Lumley, I.J. Polmear, Vacancy–solute interactions during multiple-step ageing of an Al-Cu-Mg-Ag alloy, Scripta Mater. 60 (2009) 137-140.

[49] E. Clouet, L. Laé, T. Épicier, W. Lefebvre, M. Nastar, A. Deschamps, Complex precipitation pathways in multicomponent alloys, Nature Materials. 5 (2006) 482-488.

[50] T. Malis, S.C. Cheng, R.F. Egerton, EELS log- ratio technique for specimen- thickness measurement in the TEM, J. Electron Microsc. Tech. 8 (1988) 193-200.

[51] M. Watanabe, M. Kanno, D. Ackland, C. Kiely, D. Williams, Applications of Electron Energy-Loss Spectrometry and Energy Filtering in an Aberration-Corrected JEM-2200FS STEM/TEM, Microscopy and microanalysis. 13 (2007) 1264-1265.

[52] C.C. Ahn, O.L. Krivanek, EELS Atlas Gatan Inc, 1983.

[53] E.A. Marquis, J.M. Hyde, Applications of atom-probe tomography to the characterisation of solute behaviours, Materials Science & Engineering R. 69 (2010) 37-62.

[54] E.A. Jägle, P.P. Choi, D. Raabe, The maximum separation cluster analysis algorithm for atom-probe tomography: parameter determination and accuracy, Microscopy & Microanalysis. 20 (2014) 1662-1671.

[55] J.M. Hyde, E.A. Marquis, K.B. Wilford, T.J. Williams, A sensitivity analysis of the maximum separation method for the characterisation of solute clusters. Ultramicroscopy 111 (2011) 440-447.

[56] G. Sha, H. Möller, W.E. Stumpf, J.H. Xia, G. Govender, S.P. Ringer, Solute nanostructures and their strengthening effects in Al–7Si–0.6 Mg alloy F357. Acta Materialia 60 (2012) 692-701.

[57] Y. Zhang, Z. Zhang, N.V. Medhekar, L. Bourgeois, Vacancy-tuned precipitation pathways in Al-1.7 Cu-0.025In-0.025Sb (at.%) alloy, Acta Mater. 141 (2017) 341-351.

Figure(s)

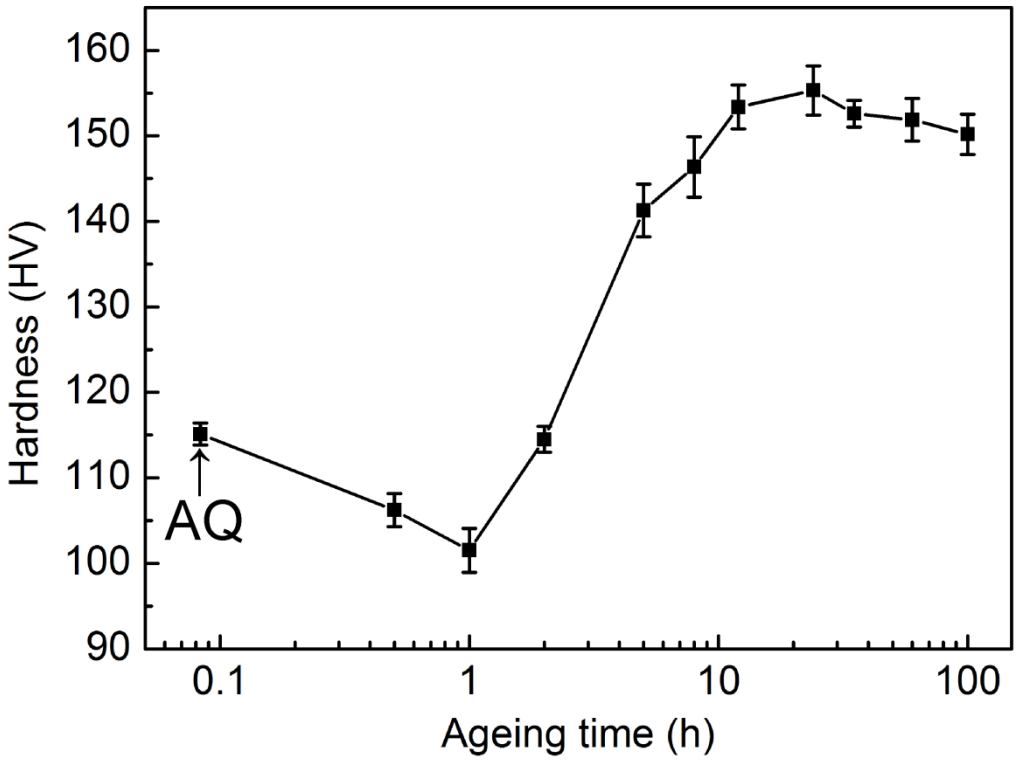

Fig. 1 Age hardening response of the Al–4.0Cu–0.3Mg–1.0Ag–0.1Si model alloy at 180 °C up to 100 h.

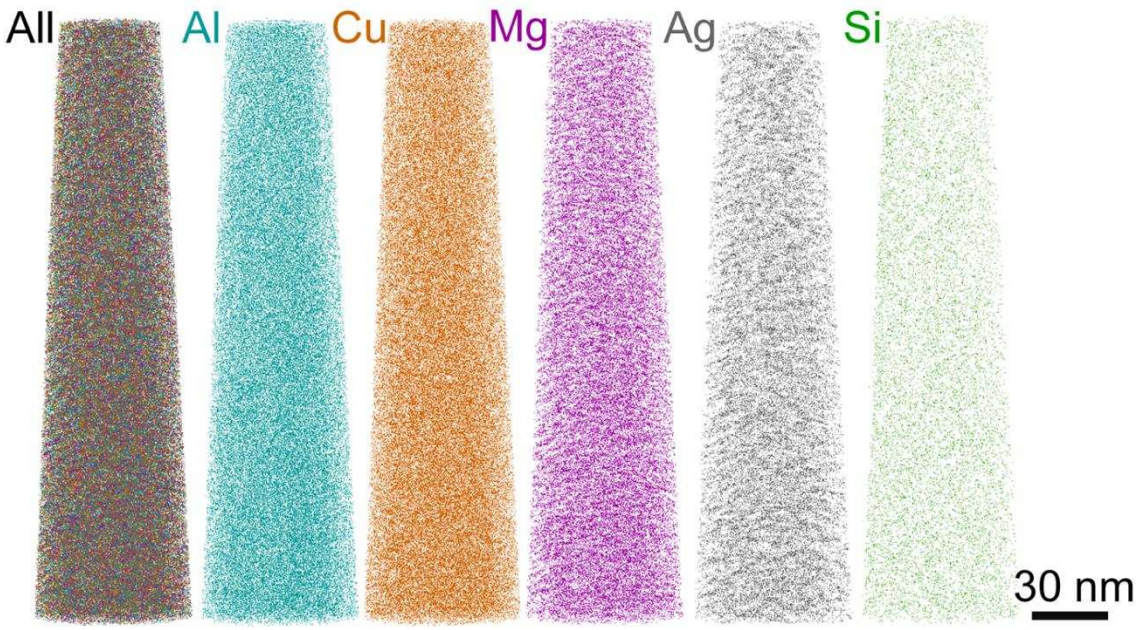

Fig. 2 3D reconstruction of atom maps with solute clusters in Al–4.0Cu–0.3Mg–1.0Ag–0.1Si alloy under AQ condition. These atom maps are shown with the raw data.

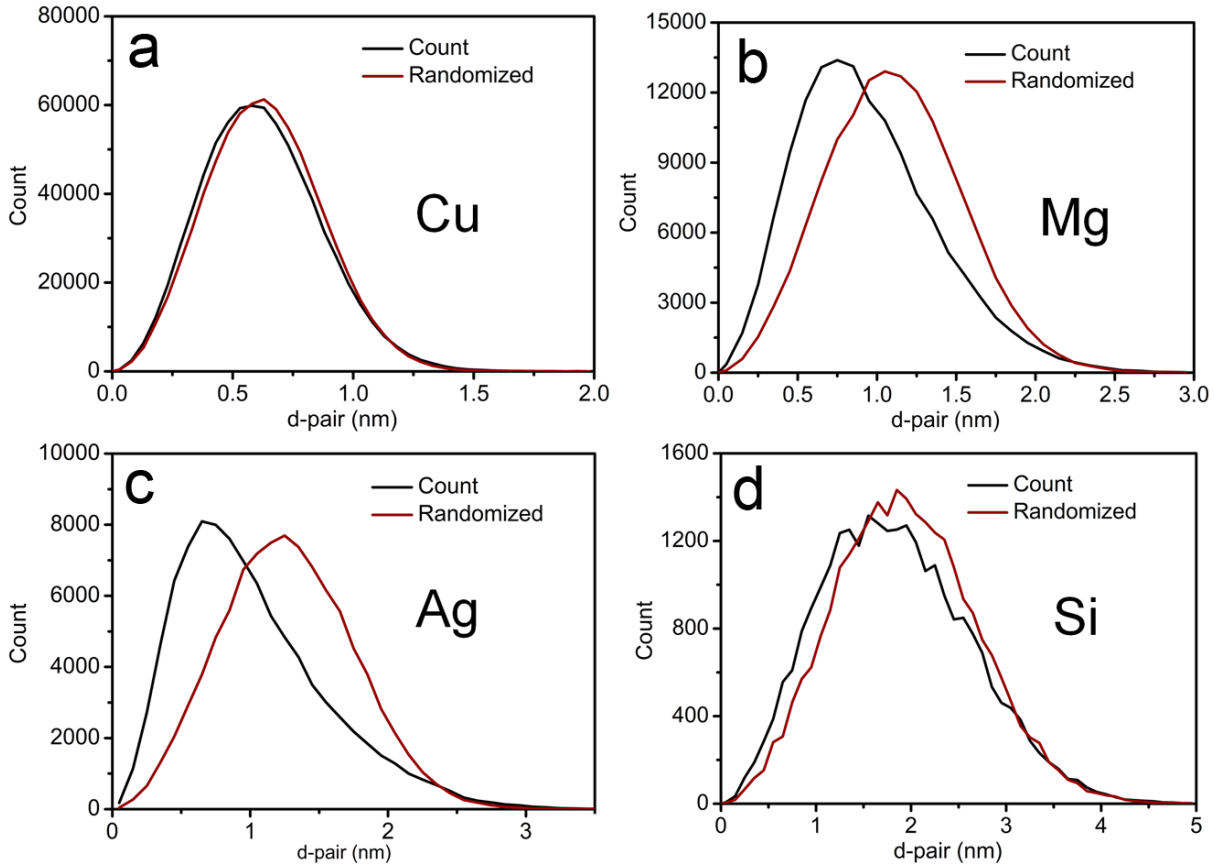

Fig. 3 The solute clustering analysis in Al–4.0Cu–0.3Mg–1.0Ag–0.1Si alloy under AQ condition. (a) Cu, (b) Mg, (c) Ag, (d) Si.

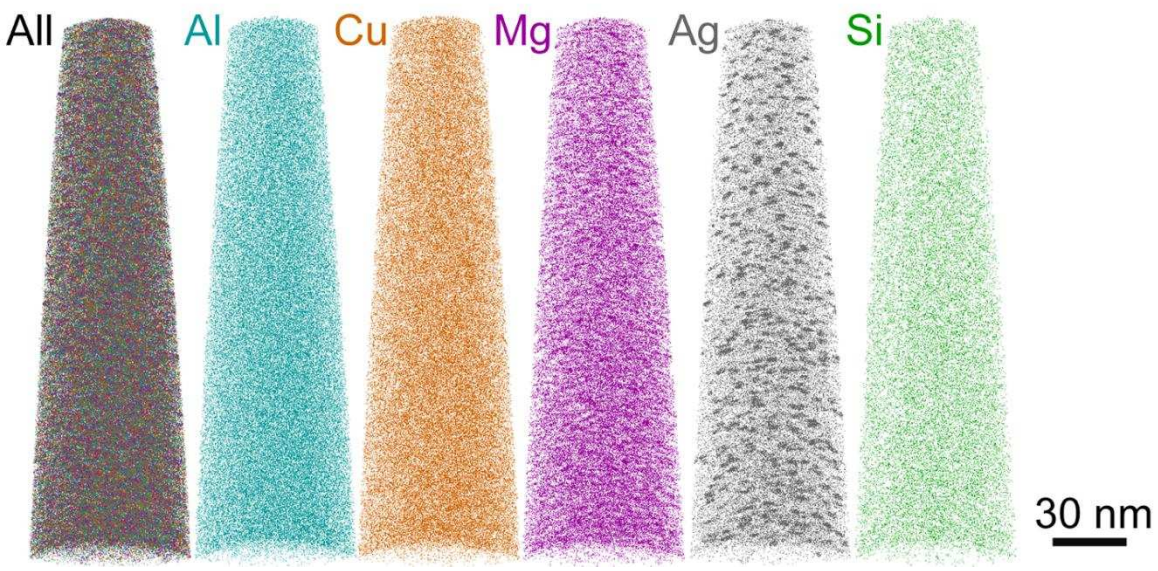

Fig. 4 3D reconstructions of atoms maps with solute clusters in Al–4.0Cu–0.3Mg–1.0Ag–0.1Si alloy aged at 180 °C for 1 h. These atom maps are shown with the raw data.

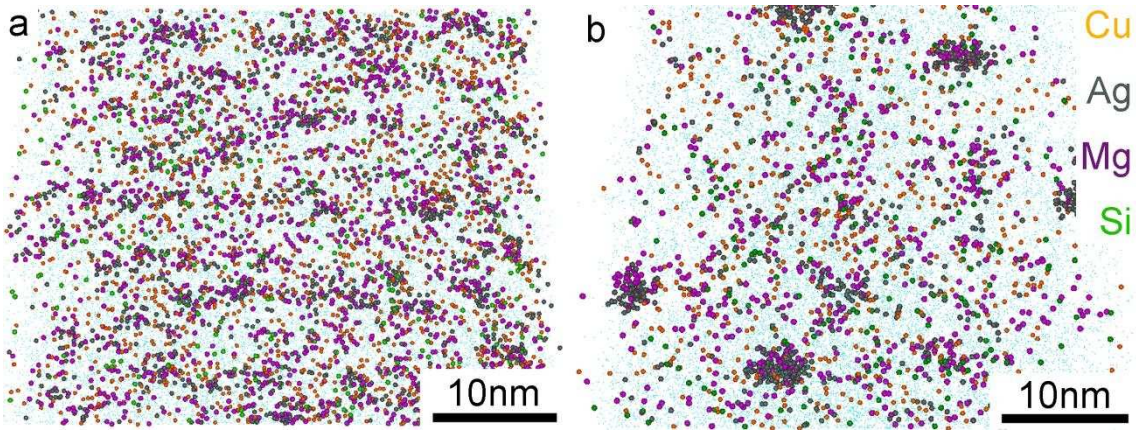

Fig. 5 Enlarged 3D reconstructions of atoms maps with solute clusters in Al–4.0Cu–0.3Mg–1.0Ag–0.1Si alloy. (a) under AQ condition, (b) aged at 180 °C for 1 h. Clearly, a significant solute clustering evolution was observed. These atom maps are shown with the raw data.

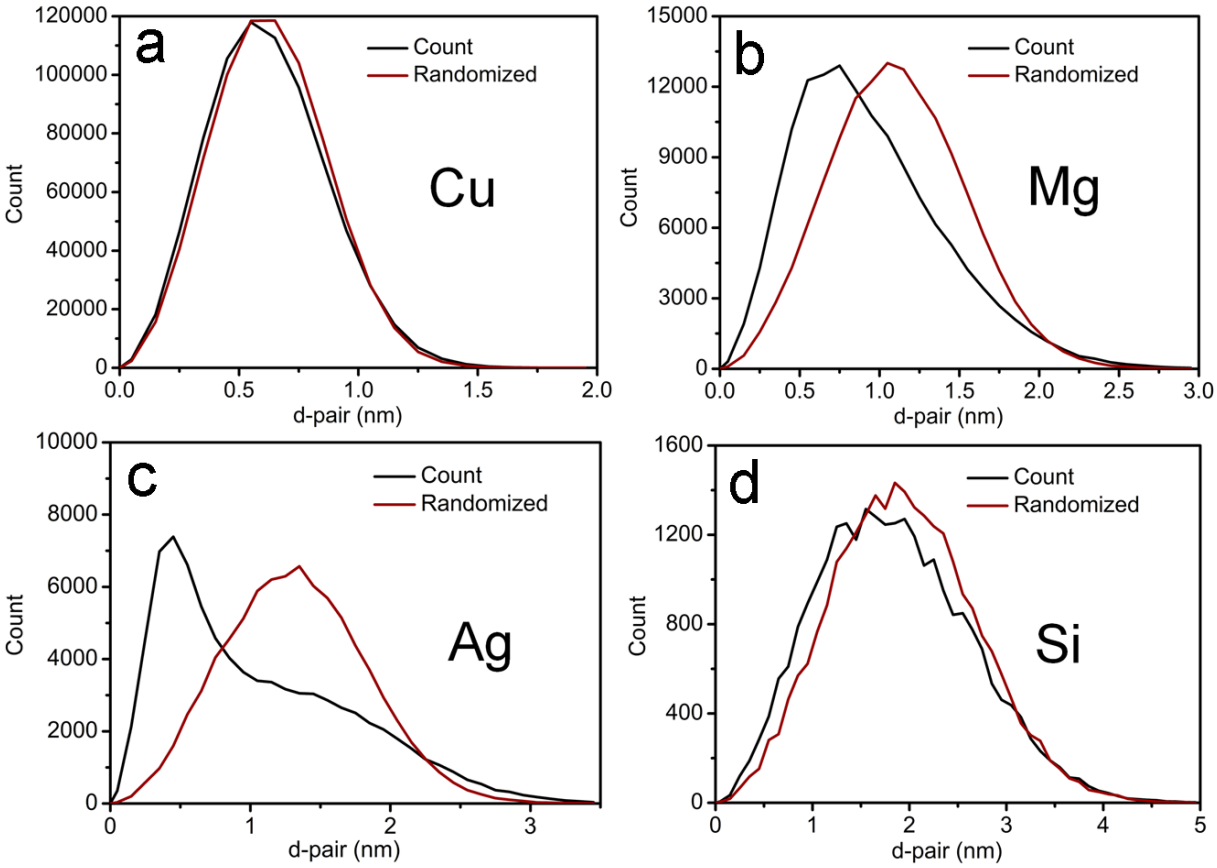

Fig. 6 The solute clustering analysis in Al–4.0Cu–0.3Mg–1.0Ag–0.1Si alloy aged at 180 °C for 1 h. (a) Cu, (b) Mg, (c) Ag, (d) Si.

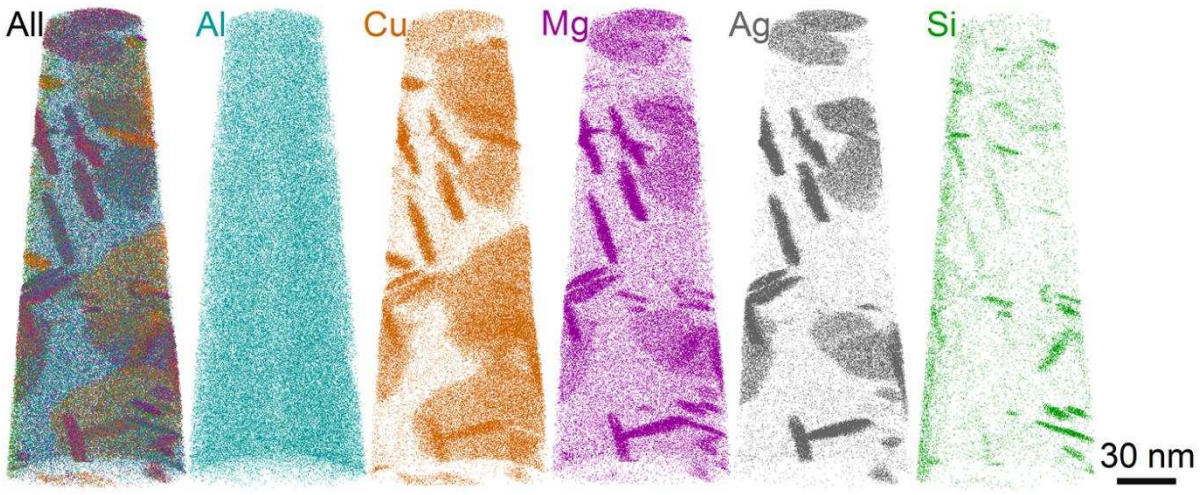

Fig. 7 3D reconstructions of atom maps with precipitates in Al–4.0Cu–0.3Mg–1.0Ag–0.1Si alloy aged at 180 °C for 24 h.

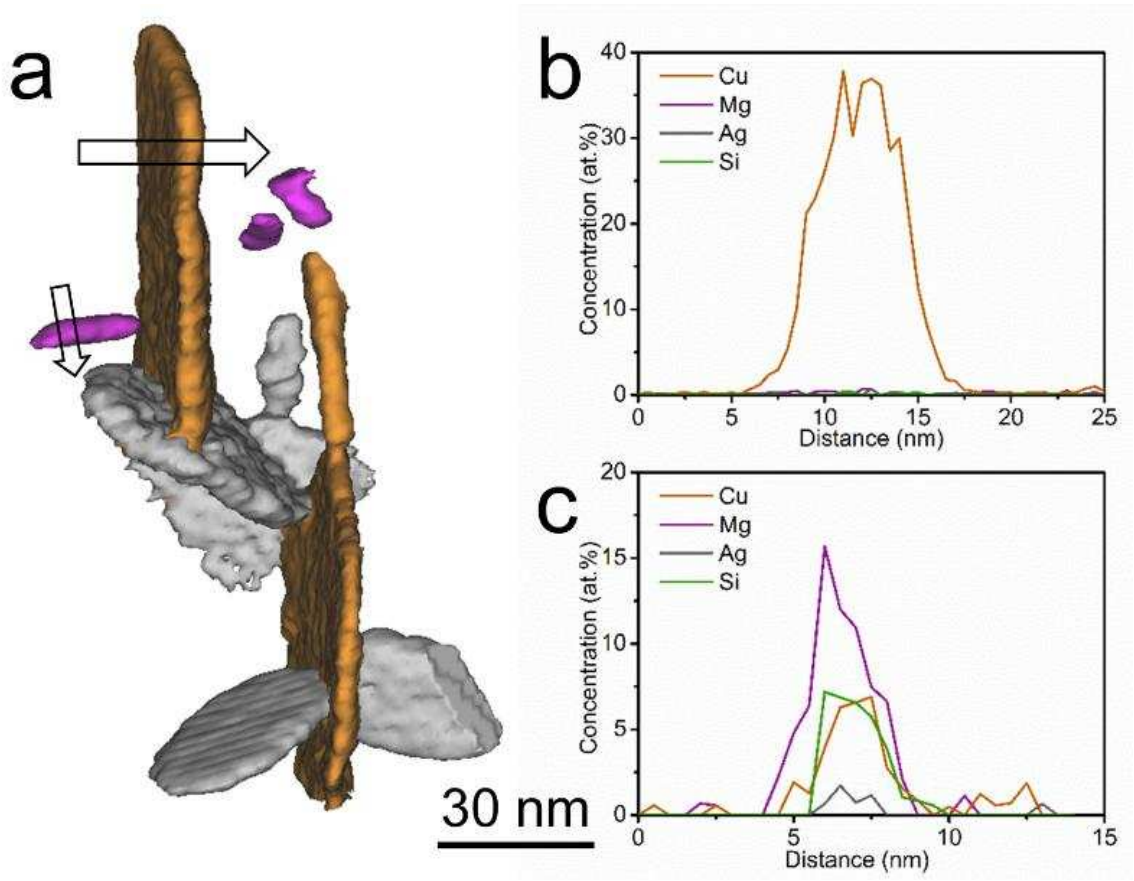

Fig. 8 (a) 3 types of precipitates (Ω (AlCuMgAg), θ (AlCu) and Mg_2Si) highlighted by isosurfaces at 1.0 at% Ag (grey), 10.0 at% Cu (orange) and 2.0 at% Mg (purple), respectively, in Al–4.0Cu–0.3Mg–1.0Ag–0.1Si alloy aged at 180 °C for 24 h. (b) 1D concentration profile measured by a cylinder of 2 nm in diameter across a θ (AlCu) precipitate marked with an arrow in (a). (c) 1D concentration profile measured by a cylinder of 2 nm in diameter across a Mg_2Si precipitate marked with an arrow in (a).

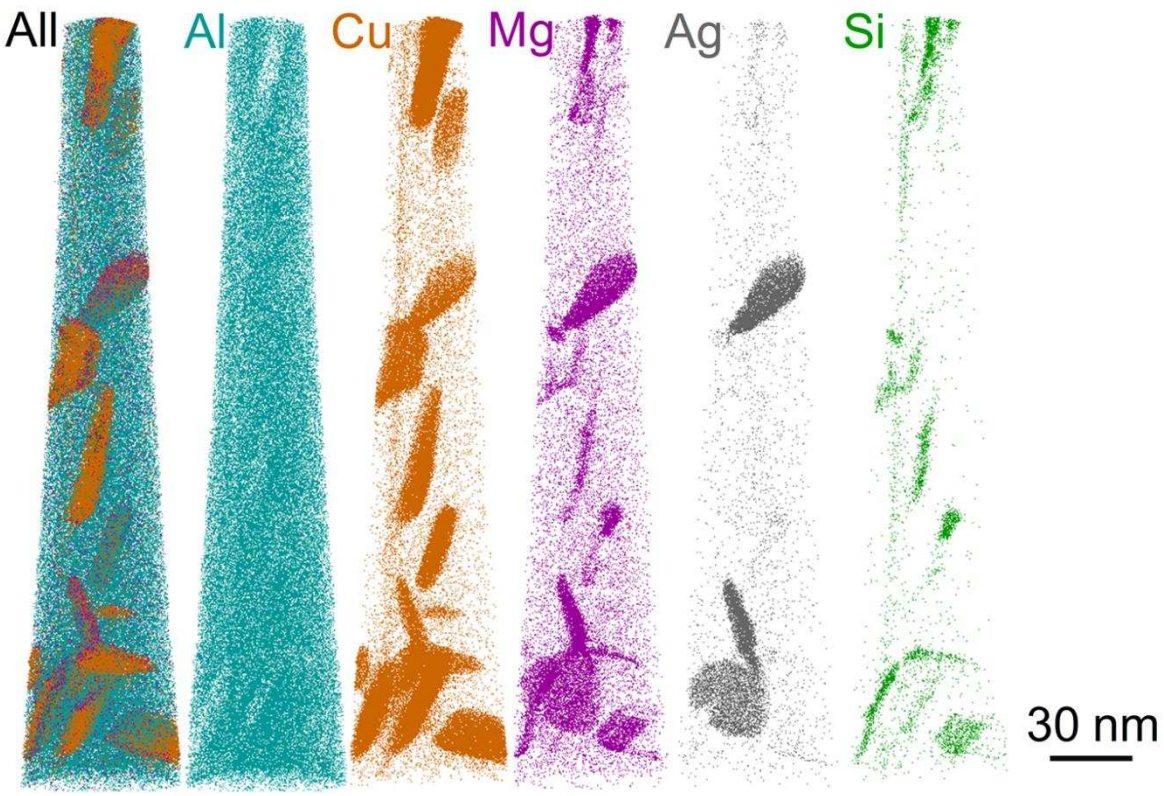

Fig. 9 3D reconstructions of atom maps with precipitates in Al–4.0Cu–0.3Mg–1.0Ag–0.1Si alloy aged at 180 °C for 100 h.

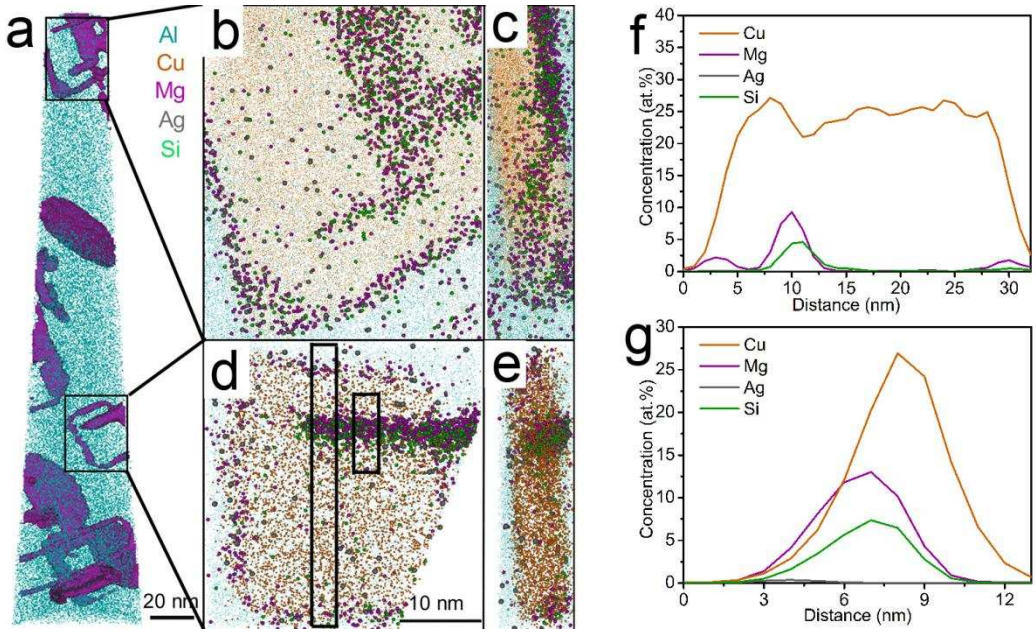

Fig. 10 (a) a 3D reconstruction of an APT dataset of Al–4.0Cu–0.3Mg–1.0Ag–0.1Si alloy aged at 180 °C for 100 h, with precipitates defined by isosurfaces at a threshold of 1.8 at% Ag, 10.0 at% Cu, 0.64 at% Mg, 2.2 at% Si. (b, c) an zoomed precipitate viewed in two different directions, as marked with one black box in (a). (d, e) another composite precipitates viewed in two different directions, as marked with a black box in (a). (f) a 1D concentration profile measured by a cylinder of 2 nm in diameter, as marked with a black long box in (d). (g) a 1D concentration profile measured by a cylinder of 2 nm in diameter, as marked with a black short box in (d).

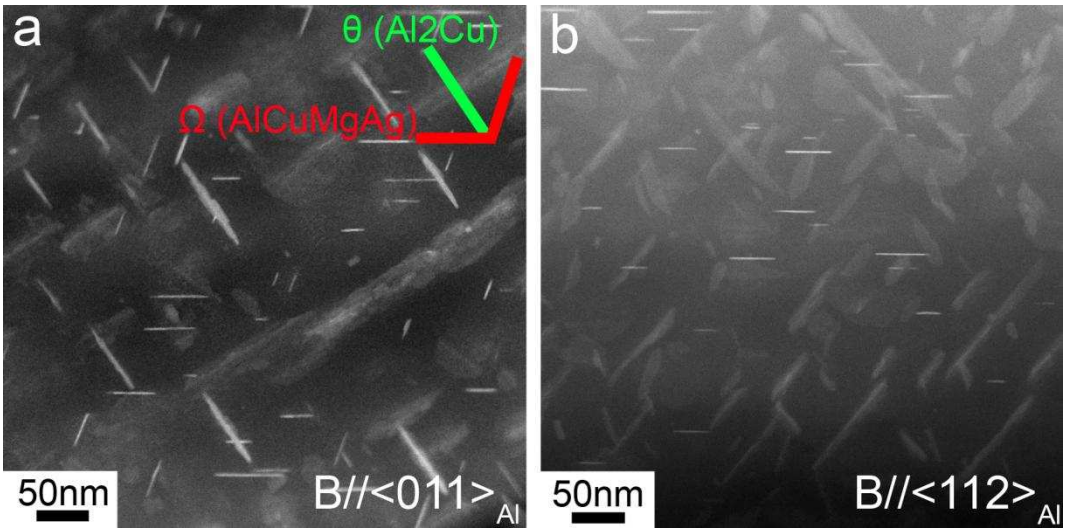

Fig. 11 Low magnification HAADF-STEM micrographs for measuring number density of the precipitates in Al–4.0Cu–0.3Mg–1.0Ag–0.1Si alloy aged at 180 °C for 24 h. The electron beam is parallel to $<011>_{Al}$ (a) and $<112>_{Al}$ (b), respectively. The habit plan of Ω (AlCuMgAg) is on $\{111\}_{Al}$ plane, as marked with red lines in (a), while the habit plan of θ (Al_2Cu)is on $\{001\}_{Al}$ plane, as marked with green lines in (a). When the sample is tilted to $<011>_{Al}$ zone axis, it is possible to determine these two different precipitates (Ω (AlCuMgAg) and θ (Al_2Cu)). However, it is not possible when the sample is tilted to $<112>_{Al}$ zone axis.

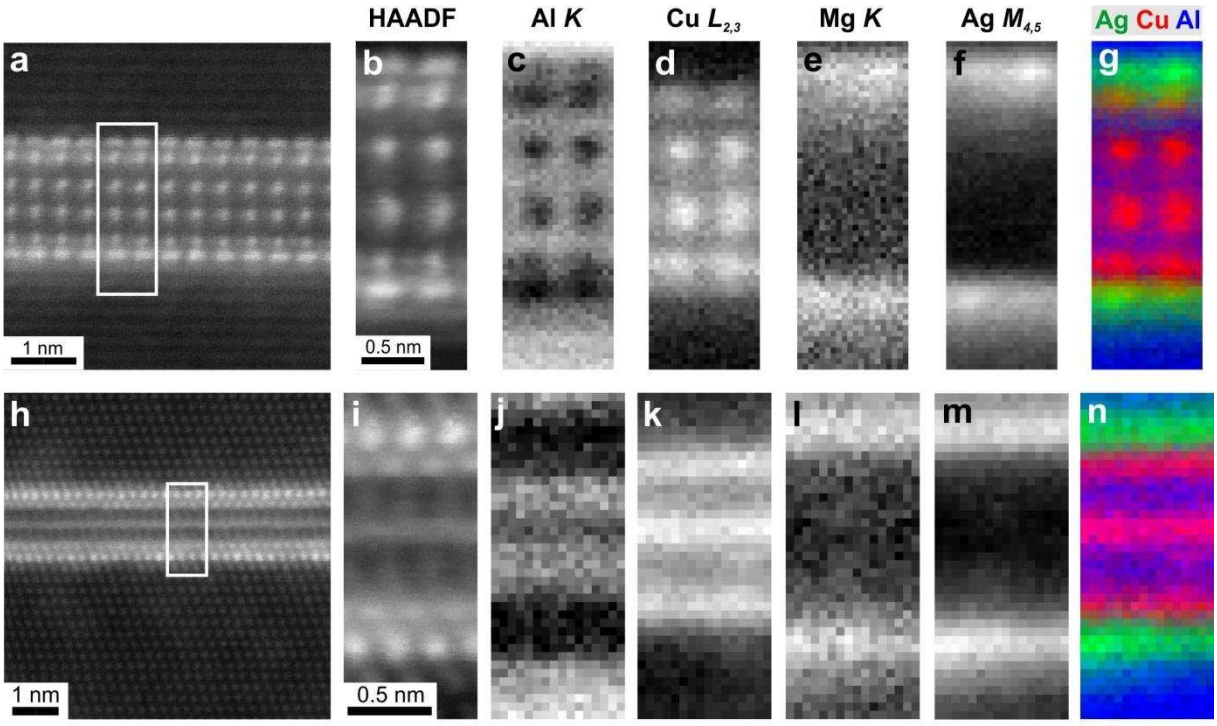

Fig. 12 (a, h) HAADF-STEM micrograph, (b, i) higher magnification HAADF-STEM micrograph of the same area as marked with a white box in (a, h), EELS elemental maps of Al (c, j), Cu (d, k), Mg (e, l), Ag (f, m) and mixed map of Cu, Mg and Ag (g, n), of the fully ordered Ω (AlCuMgAg) precipitate in Al–4.0Cu–0.3Mg–1.0Ag–0.1Si alloy aged at 180 °C for 24 h. The electron beam is parallel to $<112>_{Al}$ (a-g) and $<011>_{Al}$ (h-n), respectively.

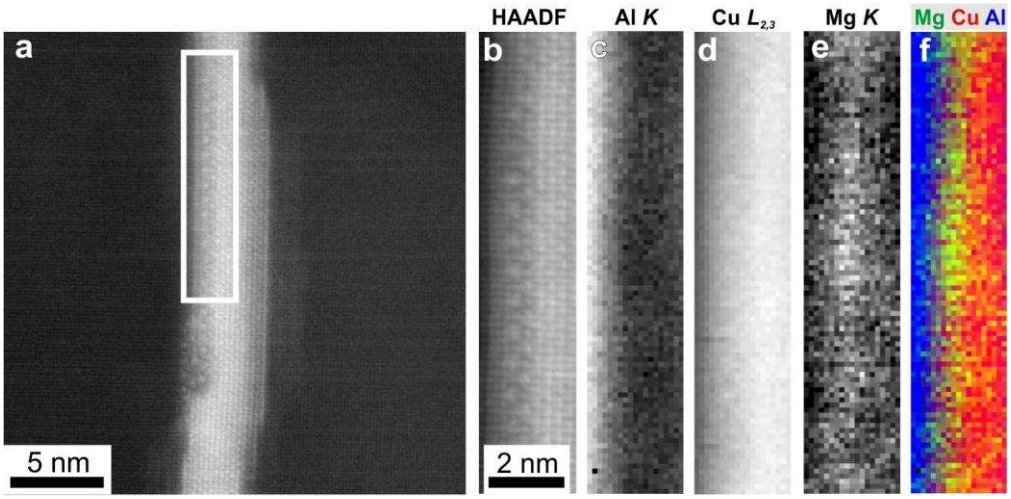

Fig. 13 (a) HAADF-STEM micrograph, (b) higher magnification HAADF-STEM micrograph of the same area as marked with a white box in (a), EELS elemental maps of Mg (c), Cu (d), and Al (e), of the Ω (AlCuMgAg) precipitate in Al–4.0Cu–0.3Mg–1.0Ag–0.1Si alloy aged at 180 °C for 100 h. The electron beam is parallel to $<001>_{Al}$.

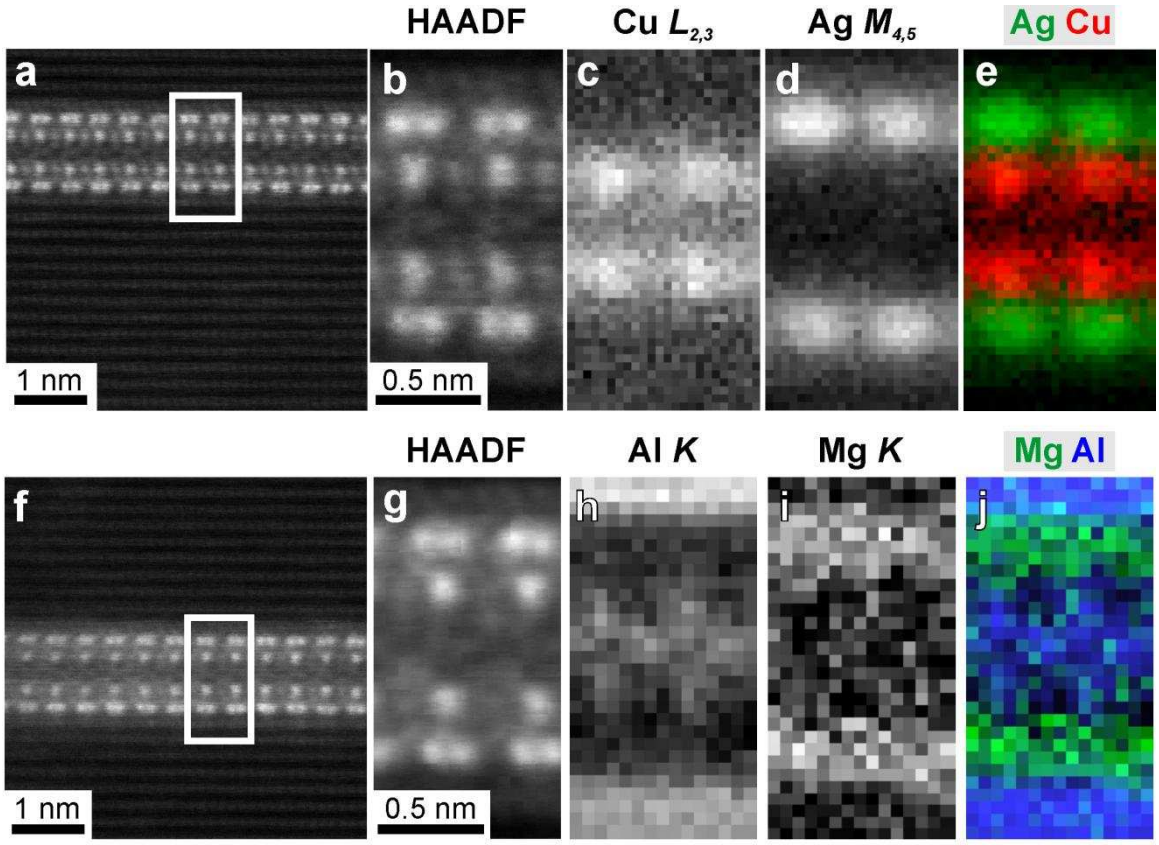

Fig. 14 (a, f) HAADF-STEM micrograph, (b, g) higher magnification HAADF-STEM micrograph of the same area as marked with a white box in (a, f), EELS elemental maps of Cu (c), Ag (d), Al (h), Mg (i) and mixed maps of Cu and Ag (e), Mg and Al (j), of the Ω (AlCuMgAg) precipitate in Al–4.0Cu–0.3Mg–1.0Ag–0.1Si alloy aged at 180 °C for 100 h. The electron beam is parallel to $<112>_{Al}$.

Table(s)

Table 1: The parameters of cluster analysis

Target elements	Parameters for cluster identification			
	d_{max} (nm)	N_{min}	L (nm)	E (nm)
Ag/Mg/Cu/Si	0.5	7	0.5	0

Table 2: Analysis of solute clusters in AQ condition and aged at 180 °C for 1 h (at. %)

Clusters	Conditions	Number of clusters	Quantity fraction (%)	Mean size (Number of solute atoms)	Error (±atoms)	Relative composition (at. %)			
						Mg	Si	Cu	Ag
Cu	AQ	93	17.88	8	3	0.00	0.00	100.00	0.00
	1 h	120	18.60	9	2	0.00	0.00	100.00	0.00
MgCu	AQ	124	23.85	9	3	21.15	0.00	78.85	0.00
	1 h	111	17.21	8	2	25.72	0.00	74.28	0.00
CuAg	AQ	50	9.62	9	3	0.00	0.00	74.12	25.88
	1 h	67	10.39	8	2	0.00	0.00	72.19	27.81
MgCuSi	AQ	18	3.46	8	1	25.71	13.57	60.71	0.00
	1 h	19	2.95	8	3	21.25	15.00	63.75	0.00
MgAgCu	AQ	181	34.81	9	3	23.09	0.00	52.86	24.05
	1 h	228	35.35	22	5	24.83	0.00	28.82	46.35
MgAgCuSi	AQ	26	5.00	10	5	22.71	11.95	42.23	23.11
	1 h	64	9.92	52	6	24.63	2.70	23.22	49.46